Add this example to Section 1.6:

Example 1.6-3. Unintended Consequence of GMO Squash

Cultivated squash plants are susceptible to a variety of viral diseases that cause infected plants to grow more slowly and produce misshapen fruits. In the mid-1990s, genetically-modified (GMO) squash that were resistant to three of the most important viral diseases were approved for release to agriculture.

Plants without the virus-resistant transgene contract the viral disease. Consequently, they do not grow as well as the GMO plants. Cucumber beetles feed on both types, but prefer the healthier GMO plants. Cucumber beetle feeding spreads bacterial wilt disease. Hence, plants resistant to viral diseases are those most likely to suffer from bacterial wilt disease. This is an example where solving problems one at a time may not be the most successful approach (Lancaster Farming, 2009).

Ref:

Lancaster Farming, 2009, Penn State Study of Modified Crop Reveals Hidden Cost of Resistance, *Lancaster Farming* 55(6):A10 (21 Nov).

Add the title of this example to the Table of Contents

Move the Bioenergetics Model, Section 1.3.7 to the end of Chapter 1. Add Section 1.9 Bioenergetics Models at the end of Chapter 1. The current Section 1.3.7 now becomes Section 1.9.1 Margaria Hydraulics Analog. Change equations numbered 1.3.21 through 1.3.26 to 1.9.1 through 1.9.6. Also, move Figure 1.3.16 to become Figure 1.9.1. Renumber the Figure number and equation numbers in the text.

1.9 Bioenergetics Models

There are a few notable bioenergetics models that are comprehensive in scope, comprising multiple steps from muscle metabolism to oxygen uptake. These take several forms, as shown in the following sections.

1.9.1 Margaria Hydraulics Model

(Insert present section 1.3.7)

1.9.2 Comprehensive Models of Exercise Metabolic Responses

A large-scale model linking oxygen uptake in the lungs with exercising skeletal muscle oxygen usage and cellular metabolism during exercise was proposed by Lai et al (2007). The overall scheme of the model appears in Figure 1.9.2, and included gas exchange in the lungs, oxygen transport by the cardiovascular system, and oxygen supplied to the muscle by the blood capillaries. Within the muscle, cellular metabolism cycled ATP to ADP by hydrolysis and ADP back to ATP by oxidative phosphorylation. Creatine and creatine phosphate were cycled as well, and metabolic water was produced from oxidative processes.

Lai et al based their model on mass transport balances, metabolic reaction balances, and equations describing exercise functions. They limited their model to oxygen only, and only indirectly accounted for the effects of carbon dioxide, pH, and glucose availability on oxygen transport and utilization. Details of lung gas exchange and cardiovascular transport were not included.

Their mass transport of oxygen began in the muscle tissue. Complete mixing of oxygen within the blood was assumed. They considered both free oxygen dissolved in the plasma and oxygen bound to hemoglobin in the red blood cells. Total oxygen available was the sum of free and bound oxygen.

The muscles were modeled as a tissue compartment and a blood capillary compartment. For each of these, the rate of oxygen storage increase or decrease (usually increasing for muscle tissue and decreasing for capillary blood) was set equal to the rate of supply (input) minus the rate of depletion (output). In general terms,

$$V \frac{dc}{dt} = \frac{d\,O_2\text{ input}}{dt} - \frac{d\,O_2\text{ output}}{dt} \qquad\qquad (1.9.7)$$

where V is volume of specific compartments in m^3; c is the oxygen concentration in kg/m^3; and t is time in sec. The oxygen input term included capillary blood flow or muscle tissue transport parameters and the oxygen output term included muscle transport and muscle utilization, depending on the compartment being described. Specific equations can be found in Lai et al (2007).

Metabolic reactions were simulated with expressions for ATP and creatine phosphate balances. Glycogenolysis and glycolysis contributions to ATP synthesis were not included. Instead, nonlinear relations between oxygen transfer and ADP and oxygen concentrations were included. These relations were largely empirical in nature.

Dynamic changes in muscle blood flow in response to a step change in exercise intensity were assumed to be exponential with a time constant of 21.3 sec for moderate exercise intensity and 24 sec for heavy exercise. Muscle blood oxygen saturation was also modeled. Muscle myoglobin dynamics do not appear to have been included.

Model representative results for muscle oxygen utilization and pulmonary oxygen uptake are given in Figure 1.9.3. The model was used to compute dynamic muscle oxygen consumption (lines) and this was compared to pulmonary oxygen uptake (symbols). It can be seen in the Figure that, at the sudden onset of very heavy exercise, muscle oxygen consumption was very rapid and of great magnitude, but pulmonary oxygen uptake lagged muscle oxygen consumption by a significant amount. This would result in predominantly anaerobic muscle metabolism and a significant transient oxygen deficit accumulation. These muscle metabolic dynamics would be difficult to monitor experimentally.

Ref:

Lai, N., M. Camesasca, G.M. Saidel, R.K. Dash, and M.E. Cabrera, 2007, Linking Pulmonary Oxygen Uptake, Muscle Oxygen Utilization, and Cellular Metabolism During Exercise, *Ann. Biomed. Engr.* 35:956-969.
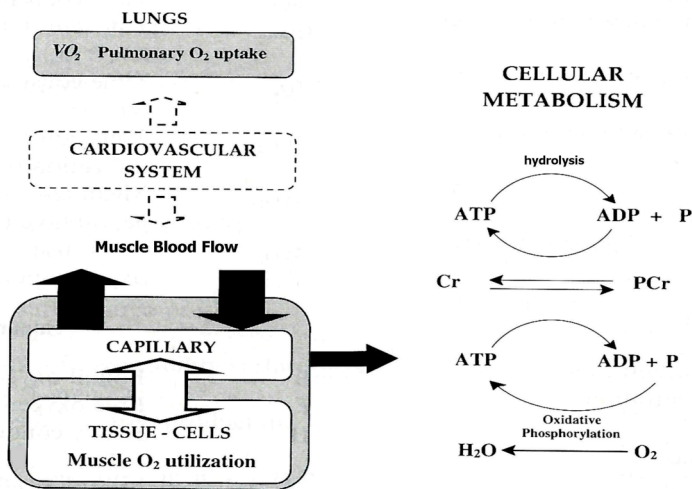
Figure 1.9.2. Schematic diagram of the Lai et al model. Oxygen enters the lungs, and is transported via the blood to the muscles. When it enters the muscle compartment, it is used to formulate ATP from ADP and creatine phosphate from creatine.
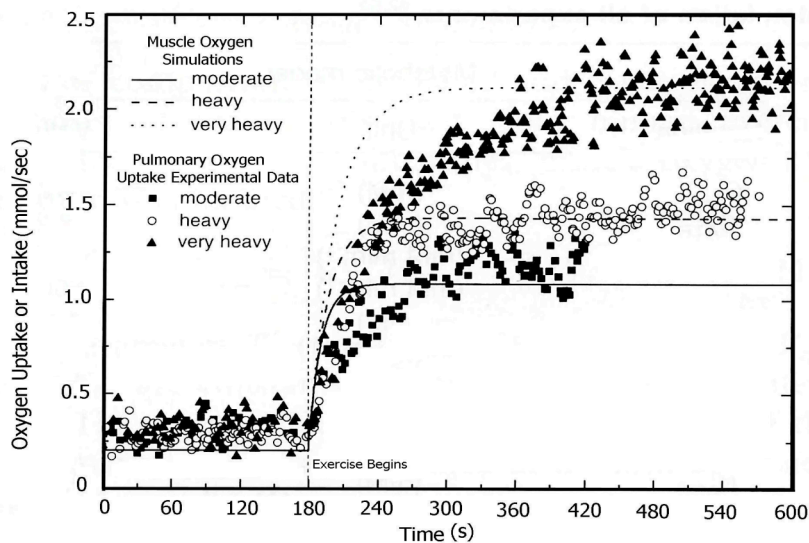

Figure 1.9.3. Results from the model compared to experimental data. Muscle oxygen use precedes lung oxygen uptake.

Figure sources:
        Fig 1.9.2 fig 1, p958 Lai et al (2007).
        Fig 1.9.3

Add to Index:

Change Table of Contents:

Remove Section 1.3.7
Add:
1.9 Bioenergetics Models
        1.9.1 Margaria Hydraulics Model
        1.9.2 Comprehensive Models of Exercise Metabolic Responses

Add to Section 3.2.2, p 140, before the paragraph beginning "Lightfoot (1974) also mentions …":

A kinetic theory based model of the Fahraeus-Lindqvist effect has been published by Gidaspow and Huang (2009). In this model, the tendency for red blood cells to flow in the center of a small tube has been confirmed through computational fluid dynamics.

Ref:

Gidaspow, D., and J. Huang, 2009, Kinetic Theory Based Model for Blood Flow and Its Viscosity, *Ann. Biomed. Engr.* 37: 1534-1545.

Add to the end of Section 3.4.3:

Arterial Pressure Model: Predicting changes in arterial pressures from one heart beat to the next was the reason an energetic model of the cardiovascular system was developed by Roytvarf and Shusterman (2008). Their model was based upon theoretical equations for conservation of mass, energy, and momentum, with esoteric mathematical expressions involving vectors and tensors. The model was intended to describe arterial pressures over a time longer than an individual heart beat, and was experimentally shown to meet this objectively successfully.

Ref:

Roytvarf, A., and V. Shusterman, 2008, A Large-Scale, Energetic Model of Cardiovascular Homeostasis Predicts Dynamics of Arterial Pressure in Humans, *IEEE Trans. Biomed. Engr.* 55(2):407-418.

Add to Index:

Add to Table of Contents, under Section 3.4.3:

Add to Section 4.2.1, p 259, between sentences beginning "Dichotomous branching …" and "After the 16th generation …":

The realization that airway branching is not as regular as Weibel has said has given rise to more realistic airway branching models to explain such things as aerosol deposition and ventilation difficulties (Ma and Lutchen, 2009; Mullally et al, 2009).

Refs:

Ma, B., and K.R. Lutchen, 2009, CFD Simulation of Aerosol Deposition in an Anatomically Based Human Large-Medium Airway Model, *Ann. Biomed. Engr.* 37: 271-285.

Mullally, W., M. Betke, M. Albert, and K. Lutchen, 2009, Explaining Clustered Ventilation Defects Via a Minimal Number of Airway Closure Locations, *Ann. Biomed. Engr.* 37: 286-300.